IDENTIFYING PLANT GENES SHAPING MICROBIOTA COMPOSITION IN THE BARLEY RHIZOSPHERE

Carmen Escudero-Martinez[1,11], Max Coulter[1,2,11], Rodrigo Alegria Terrazas[1,3], Alexandre Foito[4], Rumana Kapadia[1], Laura Pietrangelo[1,5], Mauro Maver[1,6,7], Rajiv Sharma[8], Alessio Aprile[1,9], Jenny Morris[4], Pete E. Hedley[4], Andreas Maurer[10], Klaus Pillen[10], Gino Naclerio[5], Tanja Mimmo[6,7], Geoffrey J. Barton[2], Robbie Waugh[1,4], James Abbott[2] and Davide Bulgarelli[1*]

[1]University of Dundee, Plant Sciences, School of Life Sciences, Dundee, UK; [2]University of Dundee, Computational Biology, School of Life Sciences, Dundee, UK; [3]Mohammed VI Polytechnic University, Agrobiosciences Program, Plant & Soil Microbiome Subprogram, Bengurir, Morocco; [4]The James Hutton Institute, Invergowrie, UK; [5]Department of Biosciences and Territory, University of Molise, Campobasso, Italy; [6]Faculty of Science and Technology, Free University of Bozen-Bolzano, Bolzano, Italy; [7]Competence Centre for Plant Health, Free University of Bozen-Bolzano, Bolzano, Italy; [8]Scotland's Rural College, Edinburgh, UK; [9]Department of biological and environmental sciences and technologies, University of Salento, Lecce, Italy; [10]Institute of Agricultural and Food Science and Plant Breeding, Martin Luther University, Halle-Wittenberg, Germany; [11]These authors contributed equally: Carmen Escudero-Martinez and Max Coulter.

*Correspondence: d.bulgarelli@dundee.ac.uk

Abstract

A prerequisite to exploiting soil microbes for sustainable crop production is the identification of the plant genes shaping microbiota composition in the rhizosphere, the interface between roots and soil. Here we use metagenomics information as an external quantitative phenotype to map the host genetic determinants of the rhizosphere microbiota in wild and domesticated genotypes of barley, the fourth most cultivated cereal globally. We identify a small number of loci with a major effect on the composition of rhizosphere communities. One of those, designated the *QRMC-3HS*, emerges as a major determinant of microbiota composition. We subject soil-grown sibling lines harbouring contrasting alleles at *QRMC-3HS* and hosting contrasting microbiotas to comparative root RNA-seq profiling. This allows us to identify three primary candidate genes, including a Nucleotide-Binding-Leucine-Rich-Repeat (*NLR*) gene in a region of structural variation of the barley genome. Our results provide insights into the footprint of crop improvement on the plant's capacity of shaping rhizosphere microbes.

Introduction

Plants thrive in association with diverse microbial communities, collectively referred to as the plant microbiota. This is capable of impacting the growth, development and health of their hosts[1–4]. The rhizosphere, the interface between the roots and soil[5], is a key microhabitat for the plant microbiota. For instance, similar to probiotics of the microbiota populating the digestive tract of vertebrates[6], microbes inhabiting the rhizosphere can promote plant growth by facilitating mineral nutrient uptake and pathogen protection[1,7–10].

These interactions do not represent stochastic events but are controlled, at least in part, by the plant genome[11,12]. Resolving the host genetic control of the microbes thriving at the root-soil interface therefore represents one of the prerequisites for the rational manipulation of the plant microbiota for agriculture[13]. This is particularly relevant for the microbiota associated with crop wild relatives, which, having evolved under marginal soil conditions, may represent an untapped resource for low-input agriculture[14,15]. However, despite a footprint of domestication and crop selection having been identified in the taxonomic composition of the rhizosphere microbiota in multiple plant species[16–23], host genes underpinning this diversification remain poorly understood.

Barley is the fourth-most cultivated cereal globally[24] and an attractive experimental model to study plant-microbe interactions in the light of domestication and crop selection. We previously demonstrated that wild genotypes and ‘elite’ cultivated varieties host contrasting rhizosphere microbiotas[25,26]. In this work, capitalising on an experimental population between barley genotypes at opposing ends of the domestication framework[27] and utilising state-of-the-art genomic[28] and transcriptomic[29] resources, we map host genetic determinants of microbiota composition in the rhizosphere, we identify candidate genes putatively underpinning this trait and define genetic variation occurring at those genes.

Results

The composition of the bacterial microbiota displays quantitative variation in the barley rhizosphere that appears to be controlled by a limited number of loci

We grew 52 genotypes of the progeny of a segregating population between the elite cultivar (*Hordeum vulgare ssp. vulgare*) 'Barke' and the wild ancestor accession (*Hordeum vulgare ssp. spontaneum*) called HID-144 (see Methods), hereafter designated 'elite' and 'wild' respectively, in a soil previously used for investigating the barley rhizosphere microbiota [26,30,31] under controlled environmental conditions (see Methods). At early stem elongation (Supplementary Fig. 1), plants were removed from their substrates, and the rhizosphere fractions alongside bulk soil controls were subjected to an amplicon sequencing survey of the 16S rRNA gene.

Having defined a threshold for PCR reproducibility of individual amplicon sequencing variants (ASVs) (Supplementary Fig. 2), representing the terminal taxonomic nodes in our sequencing profiling, we inspected the impact of the parental lines on the composition of the bacterial microbiota. This allowed us to identify 36 ASVs discriminating between the parental lines (Wald test, individual *P*-value < 0.05, FDR corrected, Fig. 1 a). Of these taxa, 27 ASVs, representing 5.39 % of the reads, were enriched in and discriminated between the wild genotype and the elite variety (Wald test, individual *P*-value <0.05, FDR corrected, Fig. 1 a). Conversely, 9 ASVs representing 2.74 % of the reads were enriched in and discriminated between the elite variety and the wild genotype (Wald test, individual *P*-value < 0.05, FDR corrected, Fig. 1 a). This differential microbial enrichment between the parental lines was associated with a taxonomic diversification at phylum level: while the wild-enriched profiles encompassed several ASVs classified as Bacteroidota (33.9 % of the enriched reads), Firmicutes (32.8 %), Proteobacteria (27.9 %) Acidobacteria (3.7 %) and Myxococcota (1.3 %); the elite parent enriched predominantly for members of the phylum Actinobacteria (55.8 %), followed by members of Firmicutes (17.8 %), Proteobacteria (15.3 %), Bacteroidota (10.8 %) and Acidobacteria (0.3 %) (Supplementary Fig. 3). Next, we extended our survey to the entire segregating population. We made two observations. First, and consistent with previous investigations in the same reference soil[26,30,31], rhizosphere communities were significantly different from unplanted soil controls as illustrated by sample separation along the x-axis of the Canonical analysis of Principal coordinates (CAP) (Adonis

test between bulk soil and rhizosphere samples, F = 7.49, *P*-value = 0.001, 5,000 permutations, Fig. 1 b). Despite identifying a significant impact of genotype on the composition of the rhizosphere samples, we failed to partition this variation into discrete classes (Adonis test, R^2 genotype among rhizosphere samples = 0.0403, F = 2.23, *P*-value < 0.001, 5,000 permutations, Fig. 1 b). Thus, while samples corresponding to the elite genotype segregated from the wild genotype along the y-axis accounting for the second source of variation in a constrained ordination, individual segregants were distributed between the parental lines. This distribution mirrored the increased proportion of elite genome expected in the original back-crossed BC_1S_3 population, with the majority of microbiota profiles of segregating individuals located spatially closer to the elite genotype (Fig. 1 b). These observations suggest that microbiota variation in the barley rhizosphere can be used as a trait in quantitative genetic studies.

To gain insights into the host genetic control of the rhizosphere microbiota, we developed a reductionistic approach whereby we used taxa that were differentially recruited between the parental lines and their abundances in the segregating population as “quantitative phenotypes” to search for significant associations with genetic markers located throughout the barley genome. To ascertain the phylogenetic congruence of the observed microbial trait we repeated this analysis at different taxonomic levels with sequencing reads agglomerated at genus and family level, respectively. For several bacteria we had previously characterised as being differentially abundant between the parental lines, we identified significant associations with individual homozygous or heterozygous alleles at multiple loci across the barley genome. These associations are supported either by marker regression or by a minimum LOD score of 3.43 at ASV, 3.56 at genus and 3.65 at family levels based on a LOD genome-wide significance threshold (alpha level = 0.2; 1,000 permutations) (Fig. 2, Supplementary Fig. 4-6, Supplementary Table 1 and 2, Supplementary Data 1). However, one locus that mapped between 38.7 and 40.6 centimorgans (cM) on chromosome 3H was associated with the recruitment of phylogenetically unrelated bacteria at multiple taxonomic levels. The locus was identified as *QRMC.BaH144-3HS* where *QRMC* stands for QTL–Rhizosphere Microbiota Composition, *BaH144* corresponds to the cross Barke x HID-144 and *3HS* the short arm of chromosome 3H, hereafter referred to as *QRMC-3HS*. All the

bacteria recruited at *QRMC-3HS* were significantly enriched in the wild parent. We observed up to four unrelated ASVs representing 5.68 % of the enriched bacterial reads in the parental lines were linked to the *QRMC-3HS* classified as *Variovorax sp*., *Holophaga sp*., *Sorangium sp*. and *Tahibacter sp*. When taxa were agglomerated at the genus level, the number of significant associations increased to five, including the genus Rhodanobacter. The same analysis computed at family level revealed a congruent phylogenetic pattern associated with this locus represented by Comamonadaceae (the family of the genus Variovorax), Holophagaceae (Holophaga), Polyangiaceae (Sorangium) and Rhodanobacteraceae (Rhodanobacter and Tahibacter) (Supplementary Tables 1-5). *QRMC-3HS* was the only QTL recurrently found at different taxonomic levels presenting associations with up to five taxa across analyses with a LOD threshold established with more stringent criteria (alpha level = 0.05; 1,000 permutations) (Supplementary Table 2), and explaining at least ~20 % of the phenotypic variance (*i.e*., sequencing reads) for the individual taxa significantly associated to it (Supplementary Tables 3-5). These results indicate that *QRMC-3HS* represents a major plant genetic determinant of microbiota recruitment in the barley rhizosphere.

Wild introgressions at *QRMC-3HS* are associated with compositional changes in rhizosphere bacterial microbiota

To validate the results of the mapping exercise, we tested whether barley lines harbouring contrasting alleles, *i.e.*, either ‘elite’ or ‘wild’, at *QRMC-3HS* would be associated with distinct microbial phenotypes. We generated two sibling lines designated 124_17, carrying ‘elite’ alleles at *QRMC-3HS*, and 124_52, harbouring ‘wild’ alleles at *QRMC-3HS* (Supplementary Fig. 1) by selfing the progeny of line HEB_15_124 which we identified as being heterozygous at the locus of interest (see Methods). Besides the genetic differences at *QRMC-3HS*, the derived lines share 95.5 % and 93.3 % of their genomes, respectively, with the elite parent based on molecular marker profiling using the barley 50k iSelect SNP Array[32] (Supplementary Table 6, Supplementary Data 3). They also represent *bona fide* progenies of the population investigated in this study (Supplementary Table 6).

We grew these sibling lines, along with the elite genotype and bulk soil controls, in the same experimental set-up described for the mapping experiment. We quantified

16S rRNA gene total abundance for these rhizosphere and bulk soil samples as a first step towards a comparative microbiota profiling of the new material. This quantification showed no statistical differences of 16S RNA gene total abundance among the tested genotypes (Kruskal-Wallis test, χ^2 = 12.47, and Dunn post-hoc test, *P*-value < 0.05, Supplementary Fig. 7 a). We next inspected three ecological indices of alpha diversity, *i.e.*, within sample microbial diversity, namely 'observed ASVs', 'Chao1' and 'Shannon' indices, proxies for microbiota richness and evenness. This analysis did not reveal significant differences between the communities inhabiting the rhizosphere of the sibling lines and those of the elite Barke at the threshold we imposed (ANOVA and Tukey post-hoc test, *P*-value < 0.05, Supplementary Fig. 8). Conversely, we did identify a significant host-genotype component when we inspected beta-diversity, which is the between sample microbial diversity, a proxy for microbiota composition (Adonis test, R^2 genotype = 0.119, F = 1.84, *P*-value = 0.005, 5,000 permutations). This was manifested by the separation of the communities associated with the tested genotypes, in particular those of line 124_52 (wild-like) from those of the parental line Barke along the axis accounting for the major variation in a CAP (Fig. 3 a). We were, however, unable to determine which individual ASVs were responsible for the observed differentiation at the threshold imposed in the mapping experiment (Wald test, individual *P*-value < 0.05, FDR corrected).

These results nevertheless indicate that genetic variation at *QRMC-3HS* is associated with a significant shift in community composition in the rhizosphere. This trait is not driven by 16S rRNA gene total abundance nor by differences in community richness and evenness. Despite a significant change in community composition, a wild introgression at *QRMC-3HS* is not however sufficient to trigger differential enrichments of individual bacteria.

Genetic variation at *QRMC-3HS* does not perturb the composition of the barley fungal microbiota

To investigate whether *QRMC-3HS* could shape the fungal communities inhabiting the rhizosphere, we carried out a similar sequencing survey using the rRNA ITS region. In common with the observed results for the bacterial counterpart, the evaluation of the ITS region total abundance did not reveal significant differences

194 between the sibling lines and the elite parental line Barke (Kruskal-Wallis χ^2 =
195 25.986, and Dunn post-hoc test, individual *P*-value < 0.05, Supplementary Fig. 7 b).

196 Next, we generated an amplicon sequencing library using primers targeting the rRNA
197 ITS region and identified a total of 216 fungal ASVs after applying filtering criteria
198 (see Methods). When we implemented a beta-diversity analysis of the ITS library, we
199 failed to identify a significant effect of the host genotype on these communities
200 (Adonis test, F = 0.26, *P*-value = 0.963, 5,000 permutations). This was further
201 manifested by the lack of spatial separation among microbiota samples of different
202 genotypes in a CAP (Fig. 3 b) Likewise, no differentially recruited ASVs were
203 identified in pair-wise comparisons using DESeq2 (Wald test, individual *P*-values <
204 0.05, FDR corrected).

205 These observations suggest that the selection pressure exerted by *QRMC-3HS* on
206 the barley microbiota is predominantly confined to its bacterial members.

207 ## *QRMC-3HS* does not impact other root and yield traits

208 To gain mechanistic insights into the plant traits associated with microbiota
209 diversification, we examined the root macro architecture, as morphological
210 differences in barley roots can alter microbial composition in the rhizosphere[18,30].
211 When we measured root weight and nine different root morphology parameters of
212 plants grown in the same soil used for microbiota characterisation, no significant
213 differences were found between the sibling lines and the elite genotype at the
214 imposed threshold (*i.e.*, Kruskal–Wallis and post-hoc Dunn's test, *P*-values < 0.05,
215 Supplementary Table 7).

216 Next, we grew the sibling lines and the elite genotype in sterile sand and determined
217 the elemental composition of carbon and nitrogen in their exudates, as both of these
218 elements represent another possible driver of microbial recruitment in the
219 rhizosphere[33–35]. We selected two different timepoints: 2- and 3-weeks post-
220 transplantation, to study the patterns of exudation. The former timepoint is critical for
221 the establishment of the bacterial community in cereals[36], while the latter
222 corresponds to the onset of stem elongation when the rhizosphere is harvested for
223 microbial profiling[26,30,31]. As plants were supplemented with a nutrient solution (see
224 Methods), we used wash-through from unplanted pots as controls. The carbon
225 content was significantly higher in the planted samples compared with the unplanted

ones regardless of the timepoint. For instance, unplanted samples wash-through contained just 1.5-3.6 % in carbon content weight (w/w), while that of plant exudates was 23-31 % in weight, although no significant differences among genotypes were identified at the imposed threshold (*i.e*, Kruskal–Wallis test 2 weeks, χ^2 = 12.473; Kruskal–Wallis test 3 weeks, χ^2 = 8.890 and post-hoc Dunn's test, *P*-values < 0.05) (Supplementary Fig. 9 a). No significant effect was identified among time-points, regardless of the type of specimen investigated, *i.e.*, unplanted wash-through or planted exudates (Kruskal–Wallis test, χ^2 = 17.761, *P*-value < 0.05) (Supplementary Fig. 9 b). Likewise, nitrogen content at the earliest timepoint (2 weeks) ranged from 2.8 to 6.0 % (w/w) and was not statistically different between unplanted wash-through or planted samples (ANOVA, F = 1.035, *P*-value > 0.05) (Supplementary Fig. 9 c). We could, however, differentiate among samples at the later timepoint (3 weeks), with a higher nitrogen content of 10-18 % (w/w) in the unplanted wash-through, compared to the exudates of planted samples ranging from 4-6 % (w/w) compatible with the plant's uptake of this mineral from the nutrient solution. Within these latter specimens, no significant differences among the tested genotypes were identified (Kruskal–Wallis, χ^2 = 8.567, and post-hoc Dunn's test, *P*-value < 0.05) (Supplementary Fig. 9 d).

We next explored the primary metabolism of the sibling lines and the elite genotype exudates at the onset of stem elongation stage (3 weeks) using gas chromatography–mass spectrometry (GC/MS). The metabolites recovered belong to categories such as amino acids, organic acids, carbohydrates, and other polar compounds (Supplementary Fig. 10). Amongst carbohydrates, fructose and glucose represented the largest fraction of the exudates (Supplementary Fig. 10 a). We found the majority of the compounds were classified as amino acids, with L-valine, L-leucine, L-proline, L-isoleucine, L-glutamic and L-aspartic acid as the more abundant (Supplementary Fig. 10 b). The main organic acid retrieved was succinic acid (Supplementary Fig. 10 c), while gamma-aminobutyric acid (GABA) was the most abundant in the 'other polar compounds' category (Supplementary Fig. 10 d). These compounds were present in comparable relative amounts regardless of the genotype, and the genotype effect on the metabolic composition of the exudates was not statistically significant (ANOVA and post-hoc Tukey or Kruskal–Wallis and post-hoc Dunn's test, *P*-values > 0.05, Supplementary Data 2).

To investigate any potential effect of *QRMC-3HS* on yield, we grew the sibling lines along with the elite cultivar Barke under the same conditions as the microbiota profiling to measure the thousand grain weight (TGW) and main tiller grain weight in four independent experiments (Supplementary Fig. 11). Despite a batch effect identified for one of the replicated experiments, we observed a congruent trend where the elite material had higher yield than the sibling lines, regardless of their allelic composition at *QRMC-3HS* (ANOVA TGW, F = 16.642; ANOVA main tiller grain weight, F = 20.098; post-hoc Tukey, *P*-values <0.05) (Supplementary Fig. 11). We interpret this as an indication that the *QRMC-3HS* alone may not be linked to the yield traits measured. As the sibling lines share a minor proportion (~5 %) of wild alleles at other loci, we cannot exclude a contribution of these to the yield phenotype. For instance, we identified an overlap between a yield QTL detected in the same experimental population in the pericentromeric region of chromosome 6H (43.6-52.2 cM)[37] and a region containing a wild introgression in both sibling lines (Supplementary Data 3). Likewise, genes responsible for the seed dispersal attribute of wild barley spikes, designated brittle rachis[37] (HvBtr1–HvBtr2 locus at 40,451,507 – 40,710,518 bp on chromosome 3H) map physically near to *QRMC-3HS* (33,181,340 – 36,970,860 bp on cultivar Barke) and may be implicated in the reduced yield observed in the sibling lines. We therefore used molecular markers (see Methods) to ascertain haplotype composition for these two genes. This revealed that both sibling lines and the wild parental line carry the wild alleles as they do not show mutations in *Btr1* or *Btr2* (Supplementary Fig. 12). Conversely, our elite parent Barke and four other elite lines used as controls, displayed a mutation in either of these genes, consistent with previous observations (Supplementary Fig. 12).

The sibling lines at *QRMC-3HS* and the cultivar Barke display distinct root transcriptional profiles

To further dissect the genetic mechanisms behind the differences in microbiota recruitment observed between the sibling lines 124_17 (elite-like) and 124_52 (wild-like), we conducted a comparative RNA-seq experiment using root tissue from the sibling lines and Barke. A total of 15 RNA-seq libraries were sequenced, with five biological replicates for each of the three genotypes (Supplementary Table 8). Three

291 comparisons were made: 124_52 vs Barke, 124_17 vs Barke and 124_52 vs 124_17
292 using the BaRTv2[29] Barke transcriptome as a reference.

293 Consistent with the high genotypic similarity between the sibling lines and Barke,
294 only 84 BaRTv2 genes were found to be differentially expressed (DE) in the 124_52-
295 Barke comparison, whilst 37 DE genes were identified in the 124_52-124_17
296 comparison. Interestingly, no DE genes were identified in the 124_17-Barke
297 comparison, and all but three of the DE genes identified in the 124_52-124_17
298 comparison were also found in the 124_52-Barke comparison (EdgeR, Individual *P*-
299 value < 0.01, FDR corrected, Fig. 4). These results agree with the expectation that
300 lines with the elite *QRMC-3HS* alleles (*i.e.*, the 124_17 sibling line and Barke) have
301 similar transcriptional profiles, with changes in transcription possibly reflecting
302 changes in microbiota compliment (Fig. 3)

303 A contrasting microbial phenotype was observed between the sibling lines 124_52
304 and 124_17, despite their similarity at the genetic level (Fig. 3, Supplementary Table
305 6, Supplementary Data 3). Therefore, we decided to focus on the 34 DE genes
306 shared between the 124_52-124_17 and 124_52-Barke comparisons (Fig. 4), to
307 identify gene products potentially shaping the bacterial microbiota. The full list of 34
308 DE genes is found in Supplementary Data 4. Of the 34 DE genes in the 124_52-
309 124_17 comparison, only two mapped within the *QRMC-3HS*. The first of these
310 genes is of unknown function, while the second is annotated as a nuclear binding
311 leucine-rich-repeat like (*NLR*).

312 To understand how underlying genetic differences between 124_52 and 124_17
313 related to gene expression changes, the allelic composition of these two lines were
314 compared at chromosome 3H (Fig. 5 b), and on the other 6 barley chromosomes
315 (Supplementary Fig. 13-18). We mined for regions of contrasting allelic composition
316 in each of the seven chromosomes, and once identified, these were related back to
317 the expression changes of genes expressed in the dataset (Fig. 5, Supplementary
318 Fig.13-18). We found that the majority (31 of the 34 DE genes) were found on
319 chromosome 3H, and that 28 of these were present at regions of the chromosome
320 with contrasting alleles between 124_52 and 124_17 (Fig. 5). The three DE genes
321 identified on other chromosomes were all found in regions where alleles between
322 124_52 and 124_17 do not differ. These results suggest that DE between 124_52

and 124_17 is predominantly due to cis-regulation or non-orthologous gene variation (presence/ absence variation), and that the number of trans-regulated genes is relatively small. A prediction of this observation is that differences in rhizosphere microbial phenotype between the two lines are not likely due to a large-scale reprogramming of the transcriptome. This is also reflected in the underrepresentation of differentially expressed transcription factors in the 34 124_52-124_17 DE genes (Supplementary Data 4).

Identification and prioritisation of *QRMC-3HS* candidate genes

A total of 59 genes were identified in the BaRTv2 gene/transcript[29] annotation within the bounds of the *QRMC-3HS* (identified as 33,181,340 – 36,970,860 bp on chromosome 3H in the cultivar Barke, Supplementary Data 5). Of these, 25 were found to be expressed in the RNA-seq dataset and were prioritised, as they are likely to be expressed in root tissue (Supplementary Data 5). As previously described, two out of these 25 genes were found to be DE in the 124_52-124_17 comparison subset of 34 genes (Supplementary Data 4).

To further prioritise candidate genes, variant calling was carried out to identify likely high impact and non-synonymous variants between lines 124_52 (wild-like) and 124_17 (elite-like). The variants were annotated with the BaRTv2.18 annotation using SnpEff[38]. A detailed annotation of SNPs identified in each expressed gene is shown in Supplementary Data 6. A total of 545 variants were identified across the 59 BaRTv2 genes annotated within *QRMC-3HS*. However, many of these variants were found in genes not expressed in our RNA-seq data, or were annotated as having low impact, meaning they are either synonymous changes or located in non-coding (5'/3' UTR) regions of genes and were therefore not considered as priority candidates. Two genes carried high-impact variants. BaRT2v18chr3HG123110, of unknown function, has a frameshift variant and a missing stop codon. BaRT2v18chr3HG123140, annotated as a putative Xyloglucan endotransglucosylase/hydrolase enzyme (XTH) carries a frameshift variant close to the 5' end of the coding sequence (CDS) (Supplementary Fig. 19). Fourteen other genes had moderate impact variants, all of which have missense (non-synonymous) SNPs (Supplementary Data 6).

In summary, three genes in the *QRMC-3HS* were found to either be differentially expressed between two pair-wise comparisons, *i.e.*, 124_52 vs. 124_17, and 124_52 vs. Barke, or have high impact variants and are therefore considered as primary candidates for shaping the barley rhizosphere microbiota (Supplementary Data 6).

Structural variation at *QRMC-3HS* in the barley pan-genome

The recent publication of the barley pan-genome[28] enabled us to investigate potential structural variants at *QRMC-3HS*. These may affect gene presence or expression, and therefore may impact on candidate gene prioritisation. The genome sequence for Barke is represented in the pan-genome, although our wild parent is not. We initially compared the sequence across the *QRMC-3HS* in the cultivar Barke to the corresponding sequence in the cultivar Morex (Fig. 6 a). The alignment showed conserved synteny across the *QRMC-3HS* except close to the distal end, where a region of dissimilarity of approximately 480 kb (Barke 3H: 36,582,968 – 37,063,927 bp) was identified (Fig. 6 a). To explore whether this was unique to the Barke-Morex comparison, we compared Barke to 14 other lines in the pan-genome (Supplementary Fig. 20). Comparisons of Barke with Golden Promise (Fig. 6 b), Hockett and HOR13942 (Supplementary Fig. 20) showed continuous synteny across *QRMC-3HS*, whilst the other 12 comparisons, including that with the only wild genotype in the pan-genome (B1K-04-12) showed a break in synteny similar to that observed in Morex (Fig. 6 a, Supplementary Fig. 20).

The putative *NLR* gene, BaRT2v18chr3HG123500, which was DE between 124_17 (elite-like) and 124_52 (wild-like) (Fig. 5, Supplementary Data 4), has a physical position on chromosome 3H at 36,880,423 – 36,890,887 bp, within this region of dissimilarity (Supplementary Data 4, 5, Fig. 6 a). According to the pan-genome annotation, an ortholog of this gene is not present in Morex, RGT Planet or B1K-04-12. A closer look at the counts per million of the candidate *NLR* revealed that this gene is expressed at low levels in 124_52 (Fig. 7 a).

To determine whether this low expression is due to the absence of the gene, we designed a PCR marker specific to a region of the predicted gene BaRT2v18chr3HG123500 (Fig. 7 b). We further predicted, based on sequence comparisons (Fig. 6, Supplementary Fig. 20), that the gene would be absent from Morex and RGT Planet, but present in genotypes carrying an elite *QRMC-3HS* (*i.e.*,

Barke, Hockett, Golden Promise and 124_17) and so these were included as positive and negative controls, in addition to the wild parental line HID-144. PCR results showed that an amplicon derived from the putative *NLR* gene was not detectable in RGT Planet and Morex, as anticipated from sequence comparisons, while it was present in Barke, Hockett and Golden Promise (Fig. 7 c). The amplicon was found to be present in both 124_52 (wild-like) and 124_17 (elite-like) as well as HID-144, albeit with a different size product in HID-144 and 124_52 (Supplementary Fig. 21). This suggests that the difference in *NLR* gene expression between 124_52 and 124_17 may not be due to presence/absence but other polymorphisms in its genomic sequence (Supplementary Fig. 21). Regardless, pan-genome comparisons identify the region at the distal end of the *QRMC-3HS* around the putative *NLR* as a region of sequence divergence.

Discussion

In the present study, we combined microbiota abundance and quantitative genetics to identify regions of the barley genome responsible for rhizosphere microbiota recruitment. Our results demonstrate that the taxonomic composition of the rhizosphere microbiota can be treated as a quantitative trait whose genetic basis display structural variants in the barley genome.

Our genetic mapping experiment demonstrated that the heritable component of the barley microbiota in the rhizosphere is controlled by a relatively low number of loci. This is congruent with observations of the bacterial communities inhabiting the phyllosphere of the model plant Arabidopsis[39], the staple crop maize[40] and the cereal sorghum[41]. One of the loci identified in our study, designated *QRMC-3HS*, displays an association with several phylogenetically unrelated bacteria, with the notable exception of members of Actinobacteria. While the latter are among the bacteria significantly enriched in the elite parent, as previously observed for barley plants grown in the same soil [26], no members of this phylum map at *QRMC-3HS*. A prediction from this observation is that the capacity of soil bacteria to engage with the locus *QRMC-3HS* may be evolutionarily conserved across microbial lineages. This scenario would be congruent with comparative bacterial genomics data which indicates that taxonomically diverse bacteria can share the same adaptive mechanisms to the plant environment[42,43]. An alternative, and not mutually exclusive

418 scenario, is that *QRMC-3HS* mediates the recruitment of a so-called 'microbiota
419 hubs', *i.e.*, individual microorganisms capable of regulating the proliferation of other
420 members of the community, as observed in Arabidopsis[44] and maize[45]. Mining
421 metagenome-assemblies that are significantly associated to plant loci (Oyserman *et*
422 *al*., accompanying manuscript) as well as tapping into recently developed synthetic
423 communities of the barley microbiota[46] will enable these scenarios to be investigated
424 experimentally.

425 The development of powerful genetic and genomic resources allowed us to
426 characterise *QRMC-3HS* at an unprecedented level. We made three important
427 observations. First, the sibling lines harbouring contrasting homozygous alleles at
428 *QRMC-3HS* host contrasting bacterial microbiotas. Despite these lines not triggering
429 the significant enrichment of individual taxa observed in their parental lines, our
430 approach indicates that host genetic composition is sufficient to predict an impact on
431 overall rhizosphere community structure. Besides validating our genetic mapping,
432 this observation is aligned to recent observations of sorghum genotypes[41]. Second,
433 the same lines allowed us to determine that allelic variation at *QRMC-3HS* does not
434 perturb the composition of fungal members of the community. Although this feature
435 is distinct to observations in a genome-wide investigation of root-associated
436 communities of Arabidopsis[47], our finding is consistent with recently reported results
437 for the rhizosphere microbiota of maize, where individual host genes shaped the
438 bacterial but not the fungal microbiota[10]. Third, once we characterised these lines for
439 additional traits that could be intuitively considered to be implicated in shaping the
440 microbiota in the barley rhizosphere, such as root system architecture[30] and
441 rhizodeposition of primary metabolites[48], we failed to identify significant associations
442 between these traits and allelic composition at *QRMC-3HS*. While differences in the
443 genetic background of the tested plants prevent us from drawing firm conclusions
444 when considering these studies, our observations suggest that *QRMC-3HS* may
445 code for a distinct component of the host genetic control of barley microbiota
446 recruitment.

447 We therefore employed a root RNA-seq experiment to gain mechanistic insights into
448 the regulation of the microbiota mediated by *QRMC-3HS*. One of the candidate
449 genes found to be significantly up-regulated in plants harbouring elite alleles at
450 *QRMC-3HS* putatively encodes an NLR protein[49]. This class of protein represents

one of the two main groups of immune receptors capable of selectively recognising and terminating microbial proliferation via effector recognition[50]. The gene we identified encodes a predicted protein consisting of a Rx-type coiled-coil-nucleotide-binding site-leucine-rich repeat (CC-NLR) domains, containing a putative integrated domain encompassing ankyrin repeats anchoring an NPR1-like (NONEXPRESSOR OF PATHOGENESIS-RELATED GENES 1) domain. This type of integrated *NLR* gene has recently been identified in the wheat genome[51,52]. The integrated domains may work as decoys, mimicking an effector target and enabling microbial recognition[53,54]. The *NPR1* gene is a key transcriptional regulator for plant defence responses related to the hormone salicylic acid (SA)[55]. Besides its canonical role in pathogen protection[56,57], it is important to note that *npr1* mutants, impaired in SA perception, fail to recruit a root microbiota comparable with their cognate wild-type plants[58]. A so-called resistance gene analogue sharing structural features with *bona fide NLR* genes has been identified among the candidate genes underpinning the establishment of the bacterial microbiota in sorghum[41], further suggesting the possible significance of these genes for bacterial recruitment in the rhizosphere. A distinctive feature of the *NLR* gene identified in our study is that it lies in a region of structural variation of the barley genome: for instance, the cultivar Morex, often used as a reference for microbiota investigations[25,26,31] lacks a copy of this gene. The use of the single barley reference genome available prior to 2020[59,60], would have prevented us from identifying this priority candidate gene.

Two other genes within the *QRMC-3HS* were considered among our primary candidates. The first is a gene that is differentially regulated between sibling lines harbouring contrasting microbiotas. As it encodes an unknown protein, we cannot hypothesise its mechanistic contribution to plant-microbe interactions in the rhizosphere. The second is a xyloglucan endotransglucosylase/hydrolase enzyme (XTH), characterised by a frame shift variant close to the 5' end of the CDS in the wild-like line 124_52. XTH enzymes are widely conserved across plant lineages where they are responsible for cleavage and/or re-arrangement of xyloglucans[61,62], the most abundant hemicellulosic polysaccharides in primary cell walls[63]. In Arabidopsis, cell wall features are a recruitment cue for nearly half of the endogenous root microbiota[64] and cell wall modifications underpin some of the gene ontology categories identified in genome-wide association mapping experiments

conducted with this plant[39]. A recent investigation conducted using a so-called 'split-root' approach demonstrated that genes encoding XTH were down-regulated in roots exposed to a high-density microbiome (*i.e.*, akin to natural soil conditions)[65]. Despite not identifying a significant phenotype of the macroscale root system architecture of our sibling lines, whereby XTH may play a primary role, this gene may still contribute to microbiota recruitment via modification of cell wall polysaccharides, a critical checkpoint in molecular plant-microbe interactions[66]. An additional contribution of *XTH* genes to host-microbiota interactions may be represented by an increased adaptation to soil chemical and physical conditions. For instance, *XTH* genes have previously been implicated in abiotic stress tolerance, including drought, salt stress and cold acclimation[68–70]. As wild barley accessions have evolved under marginal soil conditions, these may have imposed a selective pressure on the genetic diversity of *XTH* genes, which, in turn, may have led to a differential microbial recruitment.

As microbiota profiling has not been featuring in breeding programmes, it is legitimate to hypothesize that polymorphisms at candidate genes shaping rhizosphere microbial communities mirror a selection for other, genetically linked, agronomic traits. The observation that *QRMC-3HS* is adjacent to a major QTL for yield-related traits previously identified on chromosome 3H using the same genetic material (*QRMC-3HS*; 38.7-40.6 cM; yield QTL, 40.7-43.9 cM)[67–69] may support this scenario. Selection for yield traits may have inadvertently introduced a gene impacting the microbiota. An alternative, and not mutually exclusive, scenario is that disease resistance may have been the trait under agronomic selection. This would be in line with a recent investigation which demonstrated that bacteria isolated from the barley rhizosphere mediated the establishment of both pathogenic and mutualistic fungi in roots[73]. In this scenario, selection at *QRMC-3HS* may contribute to the fine-tuning of these multitrophic interactions. However, investigations conducted in maize indicate that plant disease resistance is not a reliable predictor of the composition of the phyllosphere microbiota[74] (*i.e.*, the microbial communities populating above-ground plant tissues), suggesting that the activity of individual genetic determinants of the microbiota may be fine-tuned by plant organ-specific mechanisms[75]. Recent innovations in barley genetics[76–79] will facilitate the

development of refined genetic material required to probe these scenarios experimentally.

In conclusion, by characterising an experimental population between wild and elite genotypes for rhizosphere microbiota composition, we have identified a putative major plant genetic determinant of the barley microbiota on chromosome 3H. Within the associated interval we have discovered three priority candidate genes, coding for an unknown function protein, an NLR and a XTH enzyme, respectively. These are putatively required for microbiota establishment in wild and cultivated barley genotypes. The latter two proteins have previously been implicated as putative regulators of the microbiota in other plant species. A striking observation derived from our investigation is that one of these candidate genes, the *NLR*, exists in a highly dynamic region of the barley genome, suggesting that selection for agronomic traits may have led to a divergent microbiota in elite cultivars. Our approach can be readily used to identify other or additional candidate genes from reference-quality genomes, including wild ancestors, as they become available for experimentation, in barley and other species. We therefore advocate the use of dedicated plant genetic resources to resolve plant-microbiota interactions at the gene level and accelerate their applications for sustainable crop production.

Methods

Plants

Barley plants from family 15 of the nested-association mapping population (NAM) HEB-25[27] were used in this investigation. We developed the sibling lines 124_52 (wild-like) and 124_17 (elite-like), with contrasting haplotypes wild and elite at the *QRMC-3HS*, by selfing the line HEB_15_124 which was heterozygous at the locus of interest. All lines used were genotyped using a combination of KASP markers and Infinium iSelect 9K and 50K SNPs arrays platforms. Barley plants used in this study along with the genetic information are summarized in Supplementary Data 3.

Plants growth conditions and rhizosphere fractionation

Barley seeds were surface sterilized and pre-germinated as previously reported[26]. Germinated seeds with comparable rootlets were sown in individual 400 mL pots filled with a sieved (15 mm) reference agricultural soil previously used for barley-

547 microbiota investigations and designated Quarryfield[26,30,31]. The number of replicates
548 varies according to the experiment: the mapping experiment n=4 for the parental
549 lines and n=2 for each of the segregating lines, whereas in the sibling lines we used
550 n=10. Unplanted soil pots were included in each experiment and designated bulk soil
551 controls. Plants were grown until stem elongation (~5 weeks, Zadoks 30–35 cereal
552 growth stage) under controlled environmental conditions as described in[31]. At this
553 developmental stage, plants were uprooted from the soil, stems were detached from
554 the uppermost 6 cm of the root system which, upon removal of large soil aggregates,
555 was subjected to a combination of washing and vortexing to dislodge rhizosphere
556 fractions as previously described[31].

557 ## Assessment of root and yield traits

558 Agronomic traits related to yield, brittle rachis and root architecture were assessed
559 for the sibling lines. Main tiller seeds grown in Quarryfield soil (n=5-8 ,4 independent
560 replicates) were used to measure yield with a MARVIN seed analyser
561 (Supplementary Fig. 11). Brittle rachis in *Btr1* and *Btr2* gene mutations were
562 assessed using KASP markers designed on *Btr* genomic sequences[78]. Root
563 architecture factors were studied for n=4 plants at early stem elongation for
564 consistency with the microbial rhizosphere experiments (Supplementary Table 7).
565 Roots were thoroughly washed and kept in phosphate buffered saline solution (PBS)
566 until processing. Root systems were scanned and analysed using WinRHIZO
567 software (Regent Instruments Inc.). Shoot and root dry weights were determined by
568 drying the samples in the oven at 70 °C for 48 h. Specific root length (cm/g) and
569 specific root area (cm^2/g) were calculated according to [18]. Normality was assessed
570 by Shapiro-Wilk test. Significance was tested with a Kruskal-Wallis or an ANOVA
571 test according to data distribution.

572 ## Barley root exudates metabolic profiling

573 We developed a protocol to characterise primary metabolites from sand-grown
574 barley plants[79] Briefly, 3 barley plantlets were sown in a 400 mL plastic pot filled with
575 approx. 300 g of pre-sterilized silver sand and organised in the glasshouse in
576 randomized blocks design (n=15 per genotype/ block). Barley nutrient solution 100
577 %[80] was applied to each pot (50 mL at 48 h intervals) and in the last week, a 25 %
578 nitrogen barley nutrient solution[80] was applied. After 2 and 3 weeks and following the

randomized block design, barley roots were carefully taken out of the pots, and the sand around the roots was washed off with water. Using a plastic jar (100 mL vol), root exudates were collected using 3 plants from the same genotype per jar. The washed plant roots were submerged in 50 mL sterilized distilled water and were left to exude for 6 to 7 h. Unplanted controls were generated by washing through the unplanted sand with sterilized distilled water collecting 50 mL, which were processed identically to the exudates. The root exudates (100 mL) and unplanted controls were collected in clean plastic jars, filtered (cellulose Whatman No. 42) and 100 µl of 2 mg/mL erythritol solution (extraction standard for GC/MS) was added to each jar. The exudate solution was frozen at -80 °C and subsequently concentrated to powder form by freeze-drying for 4 days. The experiment was harvested on four consecutive days approximately between 11 AM and 6 PM. Freeze-dried exudates (5 mg) were pooled per genotype and block (n=4) and analysed by an Elemental analyser for total carbon and nitrogen quantification using the Dumas method[81], while 20 mg of the same samples were used to perform a semiquantitative GC/MS analysis as previously described[82].

Metabolite profiles were acquired using a GC–MS (DSQII Thermo-Finnigan Tempus GC–(TOF)–MS system, UK) system carried on a DB5-MS column (15 m x 0.25 mm x 0.25 µm, J&W, Folsom, CA, USA). Data were acquired using the XCALIBUR (Thermo Scientific, Waltham, MA, USA) software package V. 2.0.7. Semiquantitative data was acquired by integrating selected ion chromatographic peaks.

Data distribution of individual compounds was assessed by Shapiro-Wilk test. Significance was tested with a Kruskal-Wallis with post-hoc Dunn test (FDR corrected) or an ANOVA test followed by a Tukey post hoc test according to data distribution.

Bacterial and fungal DNA quantification

Bacterial and fungal DNA fractions (total DNA abundance) were quantified in the rhizosphere of the sibling lines by quantitative real-time polymerase chain reaction. Rhizosphere DNA samples were diluted to 10 ng/µL and serial dilutions were applied. A final concentration of 0.1 ng/µL was employed for both the Femto Fungal DNA Quantification Kit and Femto Bacterial DNA Quantification Kit (Zymo Research) according to the manufacturer protocol. The sibling lines DNA samples were

611 randomized in 96 well plates, using a minimum of 10 biological replicates per
612 treatment. Quantification was performed in a StepOne thermocycler (Applied
613 Biosystems by Life Technology). Data distribution of the DNA samples was
614 assessed by Shapiro-Wilk test. Significance was tested with a Kruskal-Wallis with
615 post-hoc Dunn test (FDR corrected).

616 ## Preparation of 16S rRNA gene and / ITS amplicon pools and Illumina 16S rRNA and
617 ITS gene amplicon sequencing

618 16S rRNA and ITS data from the barley rhizospheres were determined using
619 previously described protocols[31]. The 515F (GTGCCAGCMGCCGCGGTAA)-806R
620 (GGACTACHVGGGTWTCTAAT) primer pair[83] were used for amplifying 16S rRNA
621 sequences, while the PCR primers ITS1F (CTTGGTCATTTAGAGGAAGTAA)-ITS2
622 (GCTGCGTTCTTCATCGATGC) were used for the ITS library[84,85]. Paired-end
623 Illumina sequencing was performed using the Illumina MiSeq system (2x 150 bp
624 reads) as indicated in [31]. Library pool quality was assessed using a Bioanalyzer
625 (High Sensitivity DNA Chip; Agilent Technologies) and quantified using a Qubit
626 (Thermo Fisher) and qPCR (Kapa Biosystems, Wilmington, USA). Amplicon libraries
627 were spiked with 15 % of a 4 pM phiX control solution. The resulting high-quality
628 libraries were run at 10 pM final concentration.

629 ## Amplicon sequencing reads processing

630 Quality assessment and DADA2 version 1.10[86] and R 3.5.1[87] was used to generate
631 the ASVs following the basic methodology outlined in the 'DADA2 Pipeline Tutorial
632 (1.10)' and it is explained in detail in[31]. Subsequently, sequences classified as
633 'Chloroplast' or 'Mitochondria' from the host plant were pruned in silico. Additional
634 pruning was carried out, removing ASVs matching a list of potential contaminants of
635 the lab[88]. Next, we merged the library used for genetic mapping with the library of the
636 sibling lines to perform simultaneous processing of both libraries creating a single
637 new Phyloseq object. Further filtering criterion was applied, low count ASVs were
638 pruned from the merged libraries (at least 20 reads in 2 % of the samples), retaining
639 93 % of the initial reads (Supplementary Fig. 1). This dataset was rarefied at equal
640 sequencing depth across samples (10500 reads) and agglomerated at genus and
641 family taxonomic levels. Finally, the resulting Phyloseq object was subsetted by the
642 corresponding library for downstream analyses.

643 The mapping 16S rRNA gene amplicon library merged with the sibling lines library
644 allowed us to identify 2,189 individual ASVs from a total of 8,219,883 sequencing
645 reads after filtering and taxonomic identification against the SILVA 138 database[89].
646 While the sibling lines ITS rRNA amplicon sequencing library was generated
647 identifying 216 individual ASVs from a total of 4,641,285 sequencing reads after
648 filtering and taxonomic identification against the Unite 04.02.2020 database[90].

649 ## Calculation of alpha-, beta-diversity indices and differential abundance between
650 rhizospheres

651 Alpha-diversity richness was estimated as described in[31]. Beta-diversity analysis was
652 carried out by calculating the dissimilarities among microbial communities using the
653 rarefied data with the Bray-Curtis index as described in[31]. For ITS, the Bray-Curtis
654 dissimilarity matrix was square-root transformed to allow visualization since all the
655 samples appeared agglomerated in the PCoA visualization. DESeq2 was used to
656 perform microbial differential abundance analysis to identify genera differentially
657 enriched between pair-wise comparisons by Wald test (False Discovery Rate, FDR <
658 0.05)[91].

659 ## QTL mapping of bacterial microbiota phenotype

660 Following the analysis of microbial differential abundance (DESeq2) between wild
661 and elite parental lines, ASVs enriched in the wild or elite parents were recapitulated
662 in the segregant population for further mapping. Association between microbial
663 abundances and loci of the barley genome was conducted using the package R/qtl[92]
664 and the function *scanone*, with the expectation-maximization (EM) algorithm
665 implementing interval mapping considering only a single-QTL model. The LOD
666 genome-wide significance threshold was set at 20 % adjusted per taxa using 1,000
667 permutations. The loci, shown in Fig. 2, were selected based on marker regression
668 analysis or their LOD scores genome adjusted per taxa (Supplementary Table 1 and
669 2) (functions *makeqtl*, *fitqtl* and *plotPXG*). The delimitation of the different loci was
670 performed by applying the Bayes credible interval method with confidence intervals
671 at 95 % (function *bayestint*[93]) (Supplementary Table 3-5). The percentage of
672 explained variance (R^2) was calculated per individual phenotype (taxa), at the
673 flanking maker of the interval upper part, corresponding to each of the individual taxa
674 mapping at this position, which is summarized in Supplementary Table 3-5.

Transcriptomic analyses (RNA-seq) of the sibling lines

Roots from the cultivar Barke and the sibling lines were processed as described above. Briefly,biological replicates of the different genotypes (n=15) were grown in a random matrix in pots filled with Quarryfield soil and maintained in the glasshouse for 5 weeks in a randomised arrangement. The uppermost 6 cm of the root system were processed as described in 'rhizosphere fractionation'. For harvesting root samples, following vortexing the root system to remove the soil/rhizosphere fractions in PBS, roots were collected with sterile forceps, excess PBS gently removed using a clean paper towel and immediately flash-frozen in liquid nitrogen until processed. All the root systems were collected in three consecutive days between 10 AM and 4 PM, reflecting the time necessary to process root samples.

RNA was extracted from individual root systems with the Macherey-Nagel™ NucleoSpin™ RNA, Mini Kit (Thermo Fisher, USA) following the manufacturer's protocol, including the Plant RNA Isolation Aid Invitrogen (Thermo Fisher, USA) for the sample lysis step using 90 µL of Plant RNA Isolation Aid, mixed with 870 µL of RA1 buffer and 40 µL of dithiothreitol (DTT). RNA quality was assessed using an Agilent 2100 Bioanalyzer or TapeStation (Agilent, USA). Samples for sequencing were selected based on microbiota profiles and the quality of the RNA sample.

Approximately, 2 µg of total RNA per sample (n=18) was submitted to Genewiz for Illumina sequencing. Total RNA (300 ng) was further purified using the NEBNext mRNA Magnetic Isolation Module (NEB). Library preparation was carried out using the NEBNext® Ultra™ II Directional RNA Library Prep with Sample Purification Beads and indexed with NEBNext Multiplex Oligos for Illumina (96 Unique Dual Index Primer Pairs set 1). Next-Generation sequencing was carried out on an Illumina NovaSeq 6000 using an SP, 300 cycles, flow cell with 2 x 150 bp paired-end reads. The library was stranded with a sequencing depth of 40 M reads per sample.

Differential expression analysis of RNA-seq

Downstream data pre-processing and analysis for both transcript quantification and variant calling was carried out using snakemake[94]. The barley reference transcriptome (v2.18) for the cultivar Barke was obtained from https://ics.hutton.ac.uk/barleyrtd/bart_v2_18.html. Raw reads were trimmed using trim galore (https://github.com/FelixKrueger/TrimGalore) version 0.6.6 with

parameters "-q 20 –Illumina –paired". Transcript quantification was carried out using Salmon[95] version 1.4.0 using parameters "-l A --seqBias –posBias –validateMappings" with BaRTv2.18[29] as the reference transcriptome. Analysis of RNA-seq quantifications was carried out using a custom modified version of the 3D RNAseq pipeline[96]. The tximport R package version 1.10.0 was used to import transcript TPM values and generate gene TPM values[97] . Low expressed transcripts and genes were filtered based on analysing the data mean-variance trend. The expected decreasing trend between data mean and variance was observed when transcripts which had < 3 of the 15 samples with counts per million reads of 2 were removed, which provided an optimal filter of low expression. A gene was counted as expressed and included in the downstream differential expression (DE) analysis if any of its transcripts met the above criteria. The TMM method was used to normalise the gene and transcript read counts to -CPM[98]. The R package umap (https://cran.r-project.org/web/packages/umap/vignettes/umap.html) implementing the umap algorithm[99] was used to visualise the expression data. It was found that sample date influenced gene expression and so this was incorporated into the EdgeR linear model as a block effect.

DE analysis was carried out using the R package EdgeR[100] version 3.32.0. The EdgeR generalised linear model quasi-likelihood (glmQL) method was used, with genotype and date of sampling used as terms in the model (~0 + genotype + sampling.date). Contrast groups were set to 124_17-Barke, 124_52-Barke and 124_52-124_17. *P*-values were corrected using the Benjamini-Hochberg method to correct the false discovery rate[101]. Genes were considered to be DE if they had an adjusted *P*-value < 0.01 and a Log2FC >=1 or <=-1 (Fig.4, 5 and Supplementary Figures 13-18).

Variant calling

For variant calling the trimmed Illumina reads were combined according to genotype (Barke, 124_17 or 124_52) using the Linux cat command (forward and reverse reads in separate files). Mapping was carried out against the barley Barke genome[28] with STAR version 2.7.9[102]. To aid with read mapping, a BaRTv2.18 gtf file was used with the "genomeGenerate" mode. After an initial round of mapping was carried out, splice junctions from each of the genotypes were collated and filtered using a custom

739 script, removing splice junctions with non-canonical dinucleotide sequences, those
740 with a read depth < 4 and a max overhang < 10 bp. The filtered splice junction set
741 was used as input for a second round of mapping.

742 Mapped read files (.bam files) were pre-processed prior to variant calling using
743 Opossum[103] with settings "SoftClipsExist True". Variant calling was carried out using
744 Platypus[104] with the barley Barke genome as a reference, and with settings "--
745 filterDuplicates 0 --minMapQual 0 --minFlank 0 --maxReadLength 500 --
746 minGoodQualBases 10 --minBaseQual 20". Variant calling files (VCF) were merged
747 using bcftools merge and filtered to remove variants outside the *QRMC-3HS* locus
748 (Barke chr3H: 33,181,340 – 36,970,860 bp). The resulting *QRMC-3HS* VCF was
749 filtered to only keep variants above the quality threshold, and where genotypes
750 Barke and 124_17 (elite-like) were called as reference alleles and 124_52 (wild-like)
751 was called as the alternative alleles. InterProScan version 5.48-83.0 (version 83.0
752 data) was used to predict functional domains of predicted proteins from transcripts.

753 ## MUMmer alignment

754 To ascertain the physical position of *QRMC-3HS* in each genome, the sequences of
755 two markers flanking the locus (*i.e.*, SCRI_RS_141171 and SCRI_RS_154747) were
756 aligned to reference genomes from the pan-genome[28] using BLAST[28,105] with default
757 parameters. The best alignment for each flanking marker was selected as the
758 physical position in each case. For the purposes of visualisation, these numbers
759 were rounded to the nearest Mb. The sequence +/- 2Mb on either side of the flanking
760 markers was extracted from each genome using a custom python script. The
761 program NUCmer from the MUMmer suite[106] was used to align the *QRMC-3HS*
762 sequence from each of the pan-genome lines against the *QRMC-3HS* sequence of
763 Barke with settings "dnadiff". The resulting delta file was filtered using delta-filter with
764 the settings "-I 95 -l 1000 -g", resulting in all alignments with less than 95 % identity
765 and lengths of less than 1,000 bp being removed. The program mummerplot was
766 then used to create figures (Fig. 6 and Supplamentary Fig. 20).

767 ## *NLR* diagnostic marker

768 The *NLR* candidate gene diagnostic PCR marker was designed to amplify the
769 flanking region of an 18 nt deletion located in the fourth intron of the predicted gene
770 in line 124_52 compared with the elite parent Barke (Supplementary Fig. 21).

Seedlings of the barley genotypes of the pangenome collection[28] were grown under controlled conditions and young leaves subjected to DNA extraction using the DNeasy Qiagen Plant Kit. The primers designated 'forward' (GCCTTTTCAGCAAGATGCCG) and 'reverse' (GTACTCCCTCCGCTCCAAAAT) were used to perform PCR amplifications with the Kapa HiFi HotStart PCR kit (Kapa Biosystems, Roche). The reactions were performed in a SimpliAmp Thermal Cycler (Applied Biosystems) using the following conditions: 94 °C (3 min), followed by 30 cycles of 98 °C (30 s) denaturing, 65 °C (30 s) annealing, 72 °C (30 s) elongation and a final elongation step of 72 °C (10 min). PCR amplicons were separated and visualised in a 2 % agarose gel (Figure 7 c).

Data Availability

The raw sequence data collected in this study have been deposited in the European Nucleotide Archive (ENA) accession number PRJEB50061. Source data to generate individual figures and computational analysis are provided with this paper. The barley reference transcriptome (v2.18) for the cultivar Barke was obtained from https://ics.hutton.ac.uk/barleyrtd/bart_v2_18.html. Pseudomolecules of individual barley genomes were downloaded from https://webblast.ipk-gatersleben.de/downloads/barley_pangenome/ .

Code Availability

The codes to reproduce the figures and statistical analyses reported in this manuscript were deposited under a DOI[107] in the GitHub repository and are accessible at https://github.com/BulgarelliD-Lab/Microbiota_mapping.

Competing interest

The authors declare no competing interests.

References

1. Berendsen, R. L. *et al.* Disease-induced assemblage of a plant-beneficial bacterial consortium. *The ISME Journal 2018 12:6* **12**, 1496–1507 (2018).

2. Hacquard, S., Spaepen, S., Garrido-Oter, R. & Schulze-Lefert, P. Interplay between innate immunity and the plant microbiota. *Annual review of phytopathology* **55**, 565–589 (2017).

3. Lu, T. *et al.* Rhizosphere microorganismscan influence the timing of plant flowering. *Microbiome* **6**, (2018).

4. Verbon, E. H. & Liberman, L. M. Beneficial microbes affect endogenous mechanisms controlling root development. *Trends in Plant Science* **21**, 218–229 (2016).

5. York, L. M., Carminati, A., Mooney, S. J., Ritz, K. & Bennett, M. J. The holistic rhizosphere: integrating zones, processes, and semantics in the soil influenced by roots. *Journal of Experimental Botany* **67**, 3629–3643 (2016).

6. Kamada, N., Chen, G. Y., Inohara, N. & Núñez, G. control of pathogens and pathobionts by the gut microbiota. *Nature immunology* **14**, 685 (2013).

7. Lugtenberg, B. & Kamilova, F. Plant-growth-promoting rhizobacteria. *Annual Review of Microbiology* **63**, 541–556 (2009).

8. Alegria Terrazas, R. *et al.* Plant-microbiota interactions as a driver of the mineral turnover in the rhizosphere. *Advances in applied microbiology* **95**, 1–67 (2016).

9. Stringlis, I. A. *et al.* MYB72-dependent coumarin exudation shapes root microbiome assembly to promote plant health. *Proceedings of the National Academy of Sciences of the United States of America* **115**, E5213–E5222 (2018).

10. Yu, P. *et al.* Plant flavones enrich rhizosphere Oxalobacteraceae to improve maize performance under nitrogen deprivation. *Nature plants* **7**, 481–499 (2021).

11. Bulgarelli, D. *et al.* Structure and functions of the bacterial microbiota of plants. *Annual Review of Plant Biology* **64**, 807-838 (2013).

12. Hacquard, S. *et al.* Microbiota and host nutrition across plant and animal kingdoms. *Cell Host and Microbe* **17**, 603–616 (2015).

13. Schlaeppi, K. & Bulgarelli, D. The plant microbiome at work. *Molecular Plant Microbe Interactions* **28**, 212–217 (2015).

14. Escudero-Martinez, C. & Bulgarelli, D. Tracing the evolutionary routes of plant-microbiota interactions. *Current opinion in microbiology* **49**, 34–40 (2019).

15. Cordovez, V., Dini-Andreote, F., Carrión, V. J. & Raaijmakers, J. M. Ecology and evolution of plant microbiomes. *Annual Review of Microbiology* **73**, 69–88 (2019).

16. Edwards, J. *et al.* Structure, variation, and assembly of the root-associated microbiomes of rice. *Proceedings of the National Academy of Sciences of the United States of America* **112**, E911–E920 (2015).

17. Leff, J. W., Lynch, R. C., Kane, N. C. & Fierer, N. Plant domestication and the assembly of bacterial and fungal communities associated with strains of the common sunflower, *Helianthus annuus*. *New Phytologist* **214**, 412–423 (2017).

18. Pérez-Jaramillo, J. E. *et al.* Linking rhizosphere microbiome composition of wild and domesticated *Phaseolus vulgaris* to genotypic and root phenotypic traits. *The ISME Journal 2017 11:10* **11**, 2244–2257 (2017).

19. Pérez-Jaramillo, J. E. *et al.* Deciphering rhizosphere microbiome assembly of wild and modern common bean (*Phaseolus vulgaris*) in native and agricultural soils from Colombia. *Microbiome* **7**, 1–16 (2019).

20. Spor, A. *et al.* Domestication-driven changes in plant traits associated with changes in the assembly of the rhizosphere microbiota in tetraploid wheat. *Scientific Reports 2020 10:1* **10**, 1–12 (2020).

21. Hassani, M. A., Özkurt, E., Franzenburg, S. & Stukenbrock, E. H. Ecological assembly processes of the bacterial and fungal microbiota of wild and domesticated wheat species. *Phytobiomes Journal* **4**, 217–224 (2020).

22. Tkacz, A. *et al.* Agricultural selection of wheat has been shaped by plant-microbe interactions. *Frontiers in Microbiology* **11**, 132 (2020).

23. Wipf, H. M. L. & Coleman-Derr, D. Evaluating domestication and ploidy effects on the assembly of the wheat bacterial microbiome. *PLOS ONE* **16**, e0248030 (2021).

24. Newton, A. C. *et al.* Crops that feed the world 4. Barley: a resilient crop? Strengths and weaknesses in the context of food security. *Food Security 2011 3:2* **3**, 141–178 (2011).

25. Bulgarelli, D. *et al.* Structure and function of the bacterial root microbiota in wild and domesticated barley resource. *Cell Host & Microbe* **17**, 392–403 (2015).

26. Alegria Terrazas, R. *et al.* A footprint of plant eco-geographic adaptation on the composition of the barley rhizosphere bacterial microbiota. *Scientific Reports 2020 10:1* **10**, 1–13 (2020).

27. Maurer, A. *et al.* Modelling the genetic architecture of flowering time control in barley through nested association mapping. *BMC Genomics 2015 16:1* **16**, 1–12 (2015).

28. Jayakodi, M. *et al.* The barley pan-genome reveals the hidden legacy of mutation breeding. *Nature 2020 588:7837* **588**, 284–289 (2020).

29. Coulter, M. *et al.* BaRTv2: A highly resolved barley reference transcriptome for accurate transcript-specific RNA-seq quantification. *bioRxiv* 2021.09.10.459729 (2021).

30. Robertson-Albertyn, S. *et al.* Root hair mutations displace the barley rhizosphere microbiota. *Frontiers in Plant Science* **8**, 1094 (2017).

31. Maver, M. *et al.* Applications of the indole-alkaloid gramine modulate the assembly of individual members of the barley rhizosphere microbiota. PeerJ **9**:e12498 (2021).

879 32. Bayer, M. M. *et al.* Development and evaluation of a barley 50k iSelect SNP
880 array. *Frontiers in Plant Science* **8**, 1792 (2017).

881 33. Bais, H. P., Weir, T. L., Perry, L. G., Gilroy, S. & Vivanco, J. M. The role of root
882 exudates in rhizosphere interactions with plants and other organisms. *Annual*
883 *Review of Plant Biology* **57**, 233–266 (2006).

884 34. Vives-Peris, V., de Ollas, C., Gómez-Cadenas, A. & Pérez-Clemente, R. M.
885 Root exudates: from plant to rhizosphere and beyond. *Plant Cell Reports 2019*
886 *39:1* **39**, 3–17 (2019).

887 35. Fagorzi, C. *et al.* Nonadditive Transcriptomic Signatures of Genotype-by-
888 Genotype Interactions during the Initiation of Plant-Rhizobium Symbiosis.
889 *mSystems* **6**, (2021).

890 36. Li, X., Rui, J., Mao, Y., Yannarell, A. & Mackie, R. Dynamics of the bacterial
891 community structure in the rhizosphere of a maize cultivar. *Soil Biology and*
892 *Biochemistry* **68**, 392–401 (2014).

893 37. Sharma, R. *et al.* Genome-wide association of yield traits in a nested
894 association mapping population of barley reveals new gene diversity for future
895 breeding. *Journal of Experimental Botany* **69**, 3811–3822 (2018).

896 38. Takahashi R, H. J. Linkage study of two complementary genes for brittle rachis
897 in barley. *Ber Ohara Inst Landwirtsch Biol Okayama Univ* **12–99**, 105 (1964).

898 39. Cingolani, P. *et al.* A program for annotating and predicting the effects of single
899 nucleotide polymorphisms, SnpEff: SNPs in the genome of *Drosophila*
900 *melanogaster* strain w1118; iso-2; iso-3. *Fly (Austin)* **6**, 80–92 (2012).

901 40. Horton, M. W. *et al.* Genome-wide association study of Arabidopsis thaliana
902 leaf microbial community. *Nature Communications 2014 5:1* **5**, 1–7 (2014).

903 41. Wallace, J. G., Kremling, K. A., Kovar, L. L. & Buckler, E. S. Quantitative
904 genetics of the maize leaf microbiome. *Phytobiomes Journal* **2**, 208–224
905 (2018).

906 42. Deng, S. *et al.* Genome wide association study reveals plant loci controlling
907 heritability of the rhizosphere microbiome. *The ISME Journal 2021 15:11* **15**,
908 3181–3194 (2021).

909 43. Bai, Y. *et al.* Functional overlap of the Arabidopsis leaf and root microbiota.
910 *Nature 2015 528:7582* **528**, 364–369 (2015).

911 44. Levy, A., Conway, J. M., Dangl, J. L. & Woyke, T. Elucidating bacterial gene
912 functions in the plant microbiome. *Cell Host & Microbe* **24**, 475–485 (2018).

913 45. Agler, M. T. *et al.* Microbial hub taxa link host and abiotic factors to plant
914 microbiome variation. *PLOS Biology* **14**, e1002352 (2016).

915 46. Niu, B., Paulson, J. N., Zheng, X. & Kolter, R. Simplified and representative
916 bacterial community of maize roots. *Proceedings of the National Academy of*
917 *Sciences of the United States of America* **114**, E2450–E2459 (2017).

47. Robertson-Albertyn, S. *et al.* A genome-annotated bacterial collection of the barley rhizosphere microbiota. *Microbiology Resource Announcements* **11**, 2 (2022) .

48. Bergelson, J., Mittelstrass, J. & Horton, M. W. Characterizing both bacteria and fungi improves understanding of the Arabidopsis root microbiome. *Scientific reports* **9**, (2019).

49. Mwafulirwa, L. *et al.* Identification of barley genetic regions influencing plant-microbe interactions and carbon cycling in soil. *Plant Soil* **468**, 165–182 (2021). .

50. van Wersch, S., Tian, L., Hoy, R. & Li, X. Plant NLRs: The whistleblowers of plant immunity. *Plant Communications* **1**, 100016 (2020).

51. Jones, J. D. G. & Dangl, J. L. The plant immune system. *Nature 2006 444:7117* **444**, 323–329 (2006).

52. Bailey, P. C. *et al.* Dominant integration locus drives continuous diversification of plant immune receptors with exogenous domain fusions. *Genome Biology* **19**, 1–18 (2018).

53. Wang, H., Zou, S., Li, Y., Lin, F. & Tang, D. An ankyrin-repeat and WRKY-domain-containing immune receptor confers stripe rust resistance in wheat. *Nature Communications 2020 11:1* **11**, 1–11 (2020).

54. Cesari, S., Bernoux, M., Moncuquet, P., Kroj, T. & Dodds, P. N. A novel conserved mechanism for plant NLR protein pairs: The “integrated decoy” hypothesis. *Frontiers in Plant Science* **5**, 25 (2014).

55. Wu, C. H., Krasileva, K. V., Banfield, M. J., Terauchi, R. & Kamoun, S. The“sensor domains”of plant NLR proteins: More than decoys? *Frontiers in Plant Science* **6**, 134 (2015).

56. Wu, Y. *et al.* The Arabidopsis NPR1 protein is a receptor for the plant defense hormone salicylic acid. *Cell reports* **1**, 639–647 (2012).

57. Chen, H. *et al.* A Bacterial Type III Effector Targets the Master Regulator of Salicylic Acid Signaling, NPR1, to Subvert Plant Immunity. *Cell Host and Microbe* **22**, 777-788.e7 (2017).

58. Zavaliev, R., Mohan, R., Chen, T. & Dong, X. Formation of NPR1 Condensates Promotes Cell Survival during the Plant Immune Response. *Cell* **182**, 1093-1108.e18 (2020).

59. Lebeis, S. L. *et al.* Salicylic acid modulates colonization of the root microbiome by specific bacterial taxa. *Science* **349**, 860–864 (2015).

60. Mayer, K. F. X. *et al.* A physical, genetic and functional sequence assembly of the barley genome. *Nature 2012 491:7426* **491**, 711–716 (2012).

61. Mascher, M. *et al.* A chromosome conformation capture ordered sequence of the barley genome. *Nature 2017 544:7651* **544**, 427–433 (2017).

957 62. Eklöf, J. M. & Brumer, H. The XTH gene family: an update on enzyme
958 structure, function, and phylogeny in xyloglucan remodeling. *Plant Physiology*
959 **153**, 456–466 (2010).

960 63. Fu, M.-M. *et al.* Genome-wide identification, characterization and expression
961 analysis of xyloglucan endotransglucosylase/hydrolase genes family in barley
962 (*Hordeum vulgare*). *Molecules 2019, Vol. 24, Page 1935* **24**, 1935 (2019).

963 64. Ezquer, I., Salameh, I., Colombo, L. & Kalaitzis, P. Plant cell walls tackling
964 climate change: biotechnological strategies to improve crop adaptations and
965 photosynthesis in response to global warming. *Plants 2020, Vol. 9, Page 212*
966 **9**, 212 (2020).

967 65. Bulgarelli, D. *et al.* Revealing structure and assembly cues for Arabidopsis
968 root-inhabiting bacterial microbiota. *Nature* **488**, 91–95 (2012).

969 66. Korenblum, E. *et al.* Rhizosphere microbiome mediates systemic root
970 metabolite exudation by root-to-root signaling. *Proceedings of the National*
971 *Academy of Sciences of the United States of America* **117**, 3874–3883 (2020).

972 67. Vorwerk, S., Somerville, S. & Somerville, C. The role of plant cell wall
973 polysaccharide composition in disease resistance. *Trends in Plant Science* **9**,
974 203–209 (2004).

975 68. Zheng, S. J. *et al.* XTH31, encoding an in vitro XEH/XET-active enzyme,
976 regulates aluminum sensitivity by modulating in vivo XET action, cell wall
977 xyloglucan content, and aluminum binding capacity in Arabidopsis. *The Plant*
978 *Cell* **24**, 4731–4747 (2012).

979 69. Takahashi, D. *et al.* Cell wall modification by the xyloglucan
980 endotransglucosylase/hydrolase XTH19 influences freezing tolerance after
981 cold and sub-zero acclimation. *Plant, Cell & Environment* **44**, 915–930 (2021).

982 70. Han, Y. *et al.* Overexpression of persimmon DkXTH1 enhanced tolerance to
983 abiotic stress and delayed fruit softening in transgenic plants. *Plant cell reports*
984 **36**, 583–596 (2017).

985 71. Nice, L. M. *et al.* Mapping agronomic traits in a wild barley advanced
986 backcross–nested association mapping population. *Crop Science* **57**, 1199–
987 1210 (2017).

988 72. Xu, X. *et al.* Genome-wide association analysis of grain yield-associated traits
989 in a pan-european barley cultivar collection. *The Plant Genome* **11**, 170073
990 (2018).

991 73. Mahdi, L. K. *et al.* The fungal root endophyte *Serendipita vermifera* displays
992 inter-kingdom synergistic beneficial effects with the microbiota in Arabidopsis
993 thaliana and barley. *The ISME Journal 2021* 1–14 (2021) doi:10.1038/s41396-
994 021-01138-y.

995 74. Wagner, M. R., Busby, P. E. & Balint-Kurti, P. Analysis of leaf microbiome
996 composition of near-isogenic maize lines differing in broad-spectrum disease
997 resistance. *New Phytologist* **225**, 2152–2165 (2020).

998 75. Munch, D. *et al.* The *Brassicaceae* family displays divergent, shoot-skewed
999 NLR resistance gene expression. *Plant physiology* **176**, 1598–1609 (2018).

1000 76. Watson, A. *et al.* Speed breeding is a powerful tool to accelerate crop research
1001 and breeding. *Nature plants* **4**, 23–29 (2018).

1002 77. Garcia-Gimenez, G. *et al.* Targeted mutation of barley (1,3;1,4)-β-glucan
1003 synthases reveals complex relationships between the storage and cell wall
1004 polysaccharide content. *The Plant journal : for cell and molecular biology* **104**,
1005 1009–1022 (2020).

1006 78. Pourkheirandish, M. et al. Evolution of the grain dispersal system in barley.
1007 undefined 162, 527–539 (2015).

1008 79. Escudero-Martinez, C., Foito, A., Kapadia, R., Aprile A. & Bulgarelli, D. Barley
1009 root exudates collection and primary metabolite profiling. DOI
1010 10.21203/rs.3.pex-1900/v1 (2022).

1011 80. Terrazas, R. A. *et al.* Nitrogen availability modulates the host control of the
1012 barley rhizosphere microbiota. *bioRxiv* 605204 (2020) doi:10.1101/605204.

1013 81. Standard operating procedure for soil total nitrogen - Dumas dry combustion
1014 method. https://www.fao.org/publications/card/en/c/CB3646EN/.

1015 82. Foito, A., Byrne, S. L., Shepherd, T., Stewart, D. & Barth, S. Transcriptional
1016 and metabolic profiles of *Lolium perenne* L. genotypes in response to a PEG-
1017 induced water stress. Plant Biotechnol Journal **8**,719-32 (2009).

1018 83. Caporaso, J. G. *et al.* Ultra-high-throughput microbial community analysis on
1019 the Illumina HiSeq and MiSeq platforms. *The ISME Journal 2012 6:8* **6**, 1621–
1020 1624 (2012).

1021 84. White, T.J., Bruns, T.D., Lee, S.B. and Taylor, J.W. Amplification and direct
1022 sequencing of fungal ribosomal RNA genes for phylogenetics. In Innis, M.A.,
1023 Gelfand, D.H., Sninsky, J.J. and White, T.J., Eds., PCR Protocols A Guide to
1024 Methods and Applications, *Academic Press*, New York, 315-322 (1990). - .

1025 85. Thompson, L. R. *et al.* A communal catalogue reveals Earth's multiscale
1026 microbial diversity. *Nature 2017 551:7681* **551**, 457–463 (2017).

1027 86. Callahan, B. J. *et al.* DADA2: High-resolution sample inference from Illumina
1028 amplicon data. *Nature methods* **13**, 581–583 (2016).

1029 87. R Core Team. R a language and environment for statistical computing. R
1030 Foundation for Statistical Computing, Vienna (Austria) (2018).

1031 88. Pietrangelo, L., Bucci, A., Maiuro, L., Bulgarelli, D. & Naclerio, G. Unraveling
1032 the composition of the root-associated bacterial microbiota of Phragmites
1033 australis and Typha latifolia. Frontiers in Microbiology 9, 1650 (2018).

1034 89. Quast C., Pruesse E., *et al.* The SILVA ribosomal RNA gene database project:
1035 improved data processing and web-based tools. Nucl. Acids Res. 41 (D1):
1036 D590-D596 (2013).

1037 90. Nilsson R.H., Larsson K.H., *et al*. The UNITE database for molecular
1038 identification of fungi: handling dark taxa and parallel taxonomic classifications.
1039 Nucleic Acids Research, DOI: 10.1093/nar/gky1022 (2018).

1040 91. Love, M. I., Huber, W. & Anders, S. Moderated estimation of fold change and
1041 dispersion for RNA-seq data with DESeq2. *Genome biology* **15**, (2014).

1042 92. Broman, K. W., Wu, H., Saunak Sen S. & Churchill, G. A. R/qtl: QTL mapping
1043 in experimental crosses. *Bioinformatics applications note* **19**, 889–890 (2003).

1044 93. Sen, Ś. & Churchill, G. A. A statistical framework for quantitative trait mapping.
1045 *Genetics* **159**, 371 (2001).

1046 94. Köster, J. & Rahmann, S. Snakemake a scalable bioinformatics workflow
1047 engine. *Bioinformatics* **28**, 2520–2522 (2012).

1048 95. Patro, R., Duggal, G., Love, M. I., Irizarry, R. A. & Kingsford, C. Salmon
1049 provides fast and bias-aware quantification of transcript expression. *Nature*
1050 *Methods 2017 14:4* **14**, 417–419 (2017).

1051 96. Guo, W. *et al.* 3D RNA-seq: a powerful and flexible tool for rapid and accurate
1052 differential expression and alternative splicing analysis of RNA-seq data for
1053 biologists. *RNA biology* **18**, 1574–1587 (2021).

1054 97. Soneson, C., Matthes, K. L., Nowicka, M., Law, C. W. & Robinson, M. D.
1055 Isoform prefiltering improves performance of count-based methods for analysis
1056 of differential transcript usage. *Genome Biology* **17**, 1–15 (2016).

1057 98. Bullard, J. H., Purdom, E., Hansen, K. D. & Dudoit, S. Evaluation of statistical
1058 methods for normalization and differential expression in mRNA-Seq
1059 experiments. *BMC Bioinformatics* **11**, 1–13 (2010).

1060 99. Mcinnes, L., Healy, J., Saul, N. & Großberger, L. UMAP: Uniform Manifold
1061 Approximation and Projection Software • Review • Repository • Archive. (2018)
1062 doi:10.21105/joss.00861.

1063 100. McCarthy, D. J., Chen, Y. & Smyth, G. K. Differential expression analysis of
1064 multifactor RNA-Seq experiments with respect to biological variation. *Nucleic*
1065 *acids research* **40**, 4288–4297 (2012).

1066 101. Benjamini, Y. & Yekutieli, D. The control of the false discovery rate in multiple
1067 testing under dependency. *Ann. Statist*. **29**, 1165–1188 (2001).

1068 102. Dobin, A. *et al.* STAR: ultrafast universal RNA-seq aligner. *Bioinformatics* **29**,
1069 15–21 (2013).

1070 103. Oikkonen, L. & Lise, S. Making the most of RNA-seq: Pre-processing
1071 sequencing data with Opossum for reliable SNP variant detection. *Wellcome*
1072 *Open Research* **2**, (2017).

104. Rimmer, A., Phan, H., Mathieson, I. et al. Integrating mapping-, assembly- and haplotype-based approaches for calling variants in clinical sequencing applications. Nat Genet **46**, 912–918 (2014)..

105. Altschul, S. F., Gish, W., Miller, W., Myers, E. W. & Lipman, D. J. Basic local alignment search tool. *Journal of molecular biology* **215**, 403–410 (1990).

106. Marçais, G. *et al.* MUMmer4: A fast and versatile genome alignment system. *PLOS Computational Biology* **14**, e1005944 (2018).

107. BulgarelliD-Lab/Microbiota_mapping: v1.22. Identifying plant genes shaping microbiota composition in the barley rhizosphere. DOI:10.5281/zenodo6584148 (2022).

Acknowledgements

We thank Malcolm Macaulay and Jim Wilde (The James Hutton Institute, Invergowrie, UK) for the technical assistance during the execution of the experiments. We also thank Nils Stein and Mary Ziems (IPK, Gatersleben, Germany) who kindly provided us with seeds of the barley pangenome collection. In addition, we thank Malcolm Macaulay and Luke Ramsay (The James Hutton Institute, Invergowrie, UK) who provided access to the diagnostic technology for Btr genes. This work was supported by a Royal Society of Edinburgh Personal Research Fellowship to DB and an UKRI grant (BB/S002871/1) to DB, GB and RW.

Author Contributions

C.E.M., R.A.T., R.W. and D.B designed the experiments. C.E.M., M.C., R.S., J.A., G.B. and D.B. conceived the data analyses. C.E.M., R.A.T., R.K., L.P., M.M, A. A., performed the experiments. C.E.M., M.C., A.F., R. K., A. A., R.S., G.N, T.M. and J.A. analysed the data. J.M. and P.H. generated the amplicon sequencing libraries. A.M and K. P. provided access to the HEB-25 seed material and analysed their genomic information. C.E.M, M.C and D.B wrote the first version of the manuscript, all authors collegially commented on and contributed to the submitted version. C.E.M and M.C contributed equally to this work.

Figure Legends

Fig. 1: Barley microbiota composition displays a quantitative variation in a segregating population between wild and elite parental lines. **a**) Ternary plot depicting microbiota composition in the elite and wild genotypes as well as bulk soil samples. Each dot illustrates an individual ASV; the size of the dots is proportional to ASV's abundance while their position reflects the microhabitat where bacteria were predominantly identified. Individual dots are colour-coded according to their significant enrichment in the rhizosphere of either parental line (Wald Test, Individual *P*-values < 0.05, FDR corrected). **b**) Canonical Analysis of Principal Coordinates computed on Bray-Curtis dissimilarity matrix. Individual dots in the plot denote individual biological replicates whose colours depict sample type in the bottom part of the figure. The number in the plot depicts the proportion of variance (R^2) explained by the factor 'Sample' within the rhizosphere microhabitat, *i.e.*, Elite, Wild or Segregant. The asterisks associated to the R^2 value denote its significance, *P*-value 'Sample' = 0.001; Adonis test, F = 2.23, 5,000 permutations. Source data are provided as a Source Data file.

Fig. 2: Genetic map of the barley determinants of individual bacterial members of the rhizosphere microbiota. Circos plot depicting **a**) the seven barley chromosomes **b**) grey connector lines link the physical position of SNPs with the genetic position in cM as indicated in the outer part of the ring; numbers in black within the individual chromosome define genetic positions (cM) significantly associated (using the function *scanone* implementing interval mapping with a single-QTL model, expectation-maximization algorithm, LOD genome-wide significance threshold 20 % adjusted per taxa, 1,000 permutations) to the differential enrichment of individual **c**) ASVs, **d**) genus or **e**) family, respectively. Different shapes depict taxonomic assignment at phylum level. Shapes are colour-coded according to the microbiota of the parental line where individual taxa were identified. Source data are provided as a Source Data file.

Fig. 3: Wild alleles at locus *QRMC-3HS* are associated with a shift in the composition of the bacterial, but not fungal, microbiota. Canonical Analysis of Principal Coordinates computed on Bray-Curtis dissimilarity matrix of **a**) bacterial or **b**) fungal ASVs' abundances. Sample type is depicted in the bottom part of the figure. The number in the plots show the proportion of variance (R^2) explained by the factors 'Batch' and 'Genotype', respectively. Asterisks associated to the R^2 value

denote its significance, ns not significant. **a**) *P*-value 'Batch' = 0.278, F = 1.10; *P*-value 'Genotype' = 0.005, F = 1.84; Adonis test 5,000 permutations. **b**) *P*-value 'Batch' = 0.027, F=3.05; *P*-value 'Genotype' = 0.963, F = 0.26; Adonis test 5,000 permutations. Source data are provided as a Source Data file.

Fig. 4: The sibling lines harbouring contrasting alleles at locus *QRMC-3HS* and the cultivar Barke display distinct root transcriptional profiles. Venn diagram showing the number of differentially expressed genes among pairs of comparisons between the sibling lines 124_52 (wild-like), 124_17 (elite-like) and their elite parent Barke (EdgeR pair-wise comparison, individual *P*-values <0.01, FDR corrected). Source data are provided as a Source Data file.

Fig. 5: Differentially expressed genes mapping at locus *QRMC-3HS*. a) Dots depict individual genes and their expression pattern in the pair-wise comparison 124_17 vs. 124_52 (log_2 Fold-Change), colour-coded according to their significance as illustrated at the bottom of the figure (EdgeR, individual *P*-values <0.01, FDR corrected). **b**) Projection of the individual genes on the structures of chromosome 3H for the lines 124_17 (elite-like) and 124_52 (wild-like), respectively, colour-coded according to allelic composition as indicated in the key at the bottom of the figure. The physical location of locus *QRMC-3HS* is highlighted in pale pink. Source data are provided as a Source Data file.

Fig. 6: Locus *QRMC-3HS* defines an area of structural variation in the barley genome. Alignment visualisation of the sequence at and surrounding the *QRMC-3HS* locus comparing **a**) the cultivars Barke and Morex and **b**) Barke to cultivar Golden Promise. The *QRMC-3HS* locus is shown in white, while purple dots represent sequencing matches longer than 1,000 bp and ≥ 95 % identity. The gap in the diagonal in **a**) denotes a disruption of synteny between the two genotypes. Numbers on the axis denote the physical interval, in bp, analysed in the given genomes. Source data are provided as a Source Data file.

Fig. 7: The *NLR* gene associated with genotype-dependent transcriptional and genomic variations. a) Boxplot showing the root RNA-seq *NLR* expression across the elite and the sibling lines in normalized counts per million. Individual dots depict individual biological replicates. Upper and lower edges of the box plots represent the upper and lower quartiles, respectively. The bold line within the box denotes the

1171 median. Whiskers denote values within 1.5 interquartile ranges. **b**) Schematic
1172 representation of the *NLR* gene transcripts inferred from the RNA-seq data depicting
1173 predicted protein domains from InterProScan. The black arrow depicts the predicted
1174 amplicon site of the PCR marker **c**) PCR amplicons partially covering the intron
1175 between the LRR and the ankyrin domains in the indicated genotypes-Negative
1176 control (NC). A DNA ladder was loaded in the first and last well of each lane,
1177 arrowheads indicate the 200 bp fragment. The diagnostic screening was repeated
1178 twice with identical results. Source data are provided as a Source Data file.

Fig.1: Microbiota composition displays a quantitative variation in a barley segregant population between wild and elite parental lines

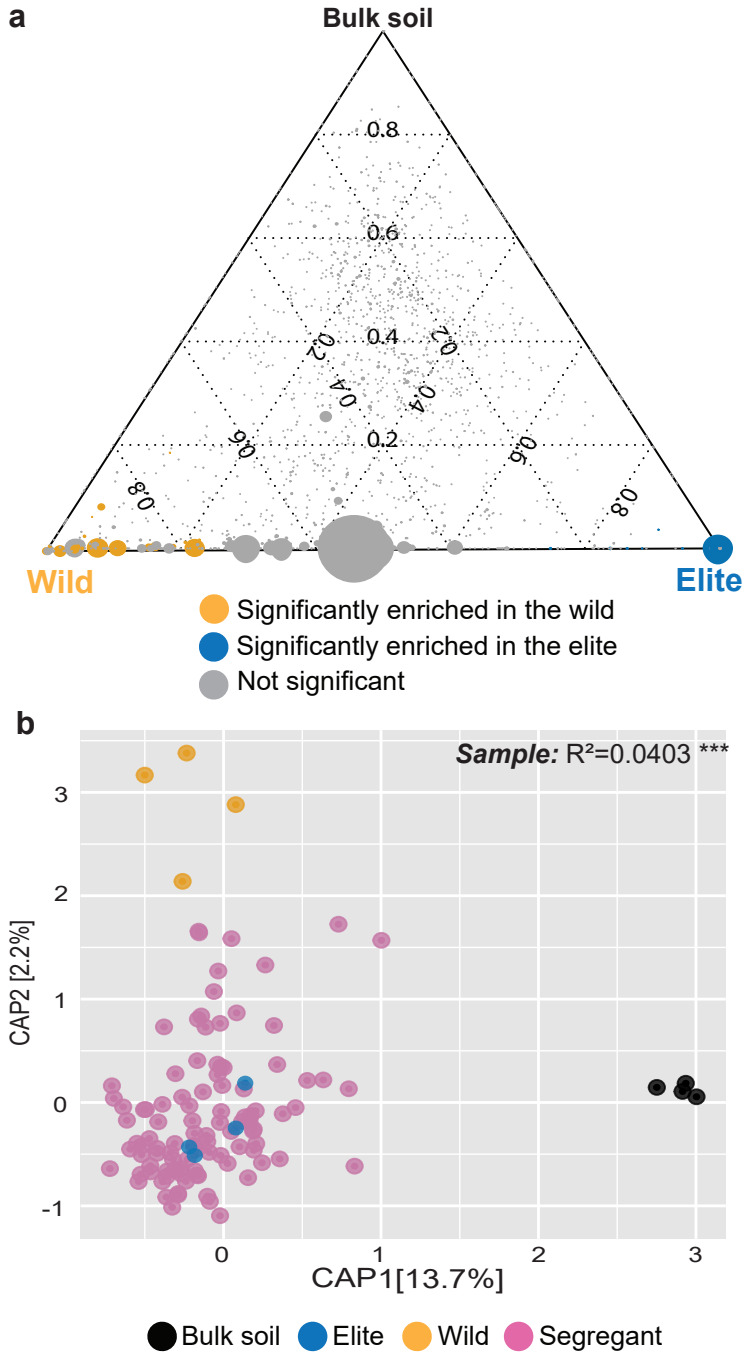

Fig.2: Genetic map of the barley determinants of individual bacterial members of the rhizosphere microbiota

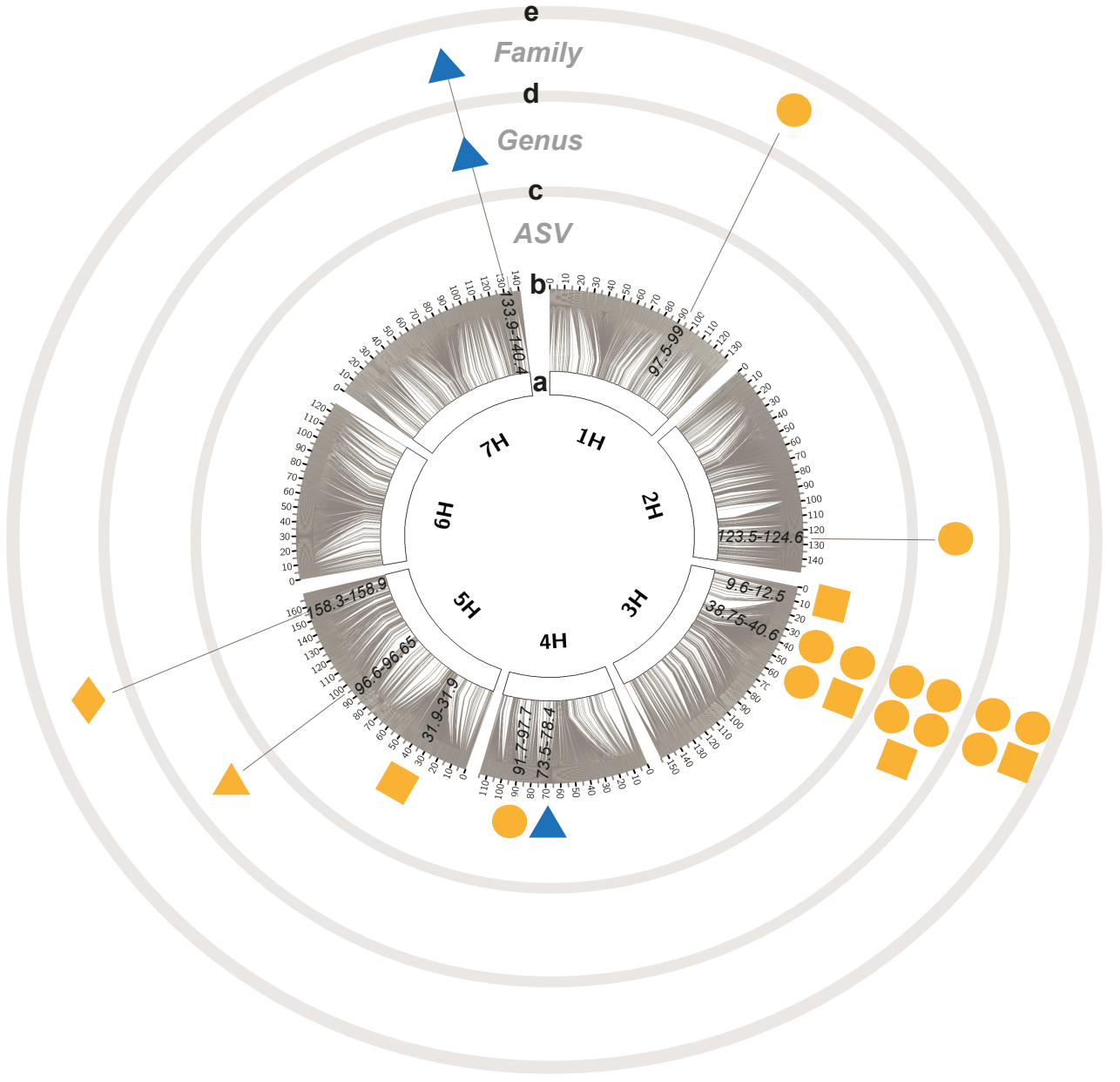

Enriched in wild Enriched in elite

Taxonomy

Proteobacteria Actinobacteria Acidobacteria Bacteroidota

Fig. 3 : Wild alleles at locus *QRMC-3HS* are associated to a shift in the composition of the bacterial, but not fungal, microbiota

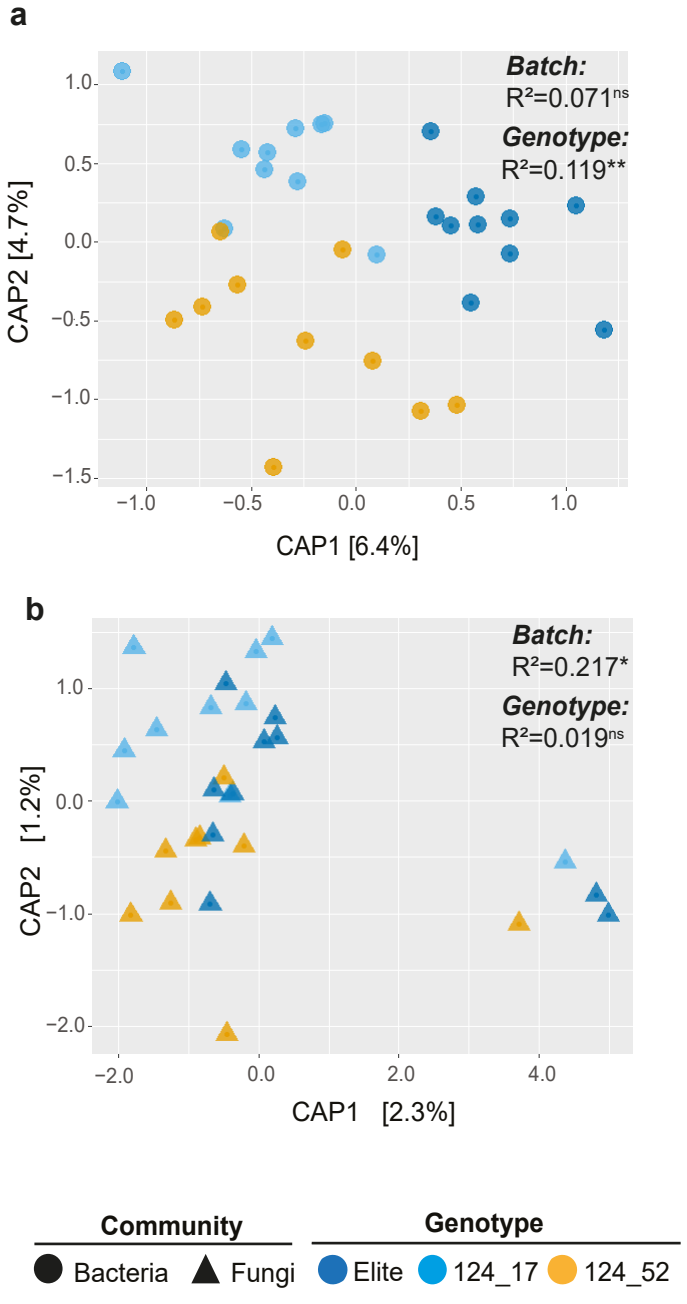

Fig. 4: Sibling lines harboring contrasting alleles at locus *QRMC-3HS* and the cultivar Barke display distinct root transcriptional profiles

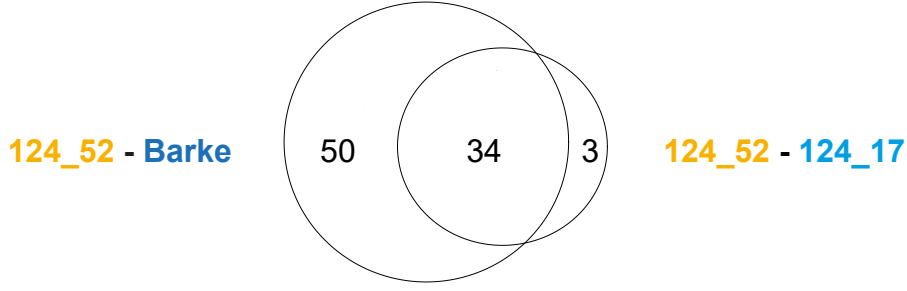

Fig. 5: Differentially expressed genes mapping at locus *QRMC-3HS*

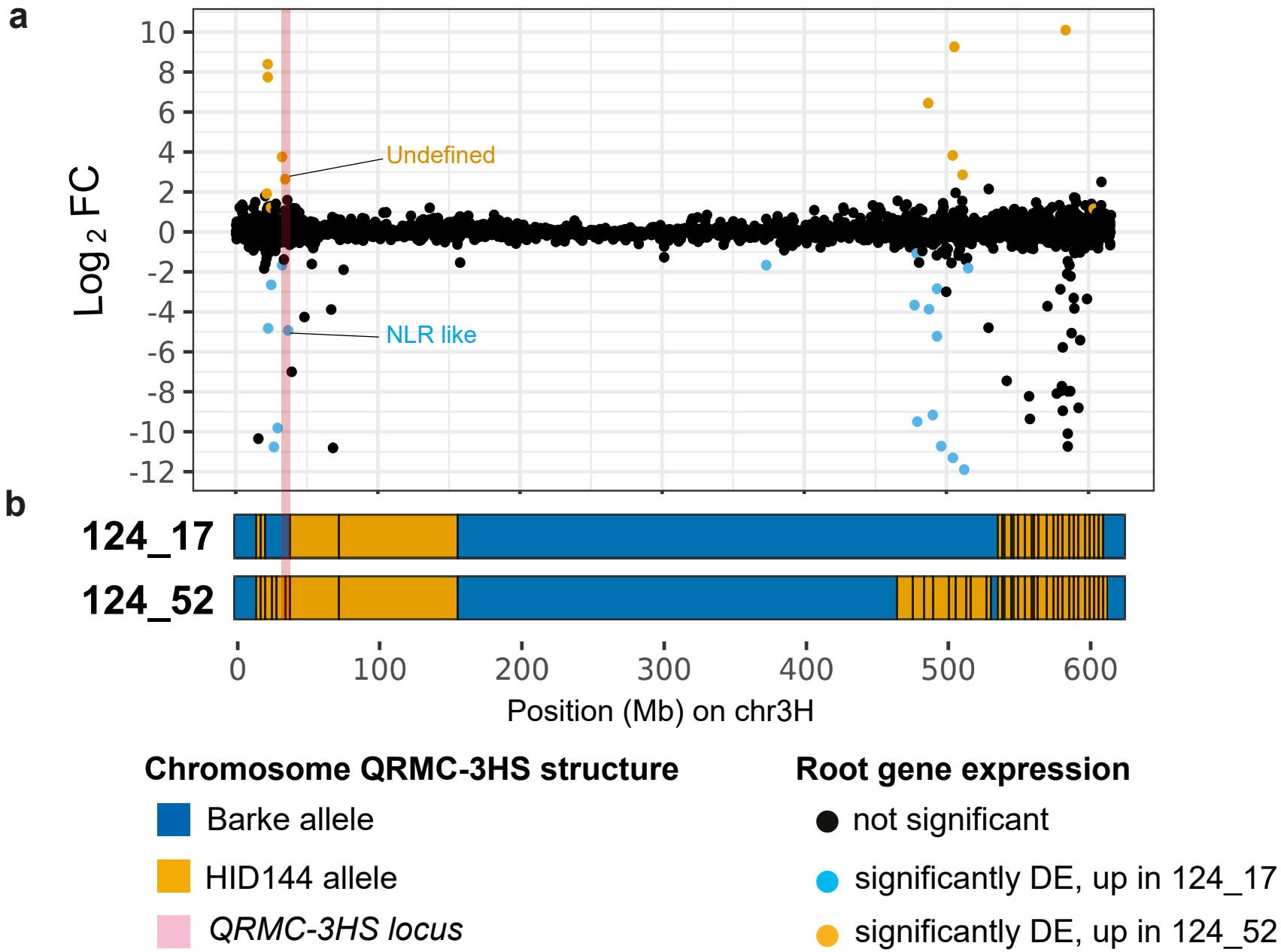

Fig. 6 : Locus *QRMC-3HS* defines an area of structural variation in the barley genome

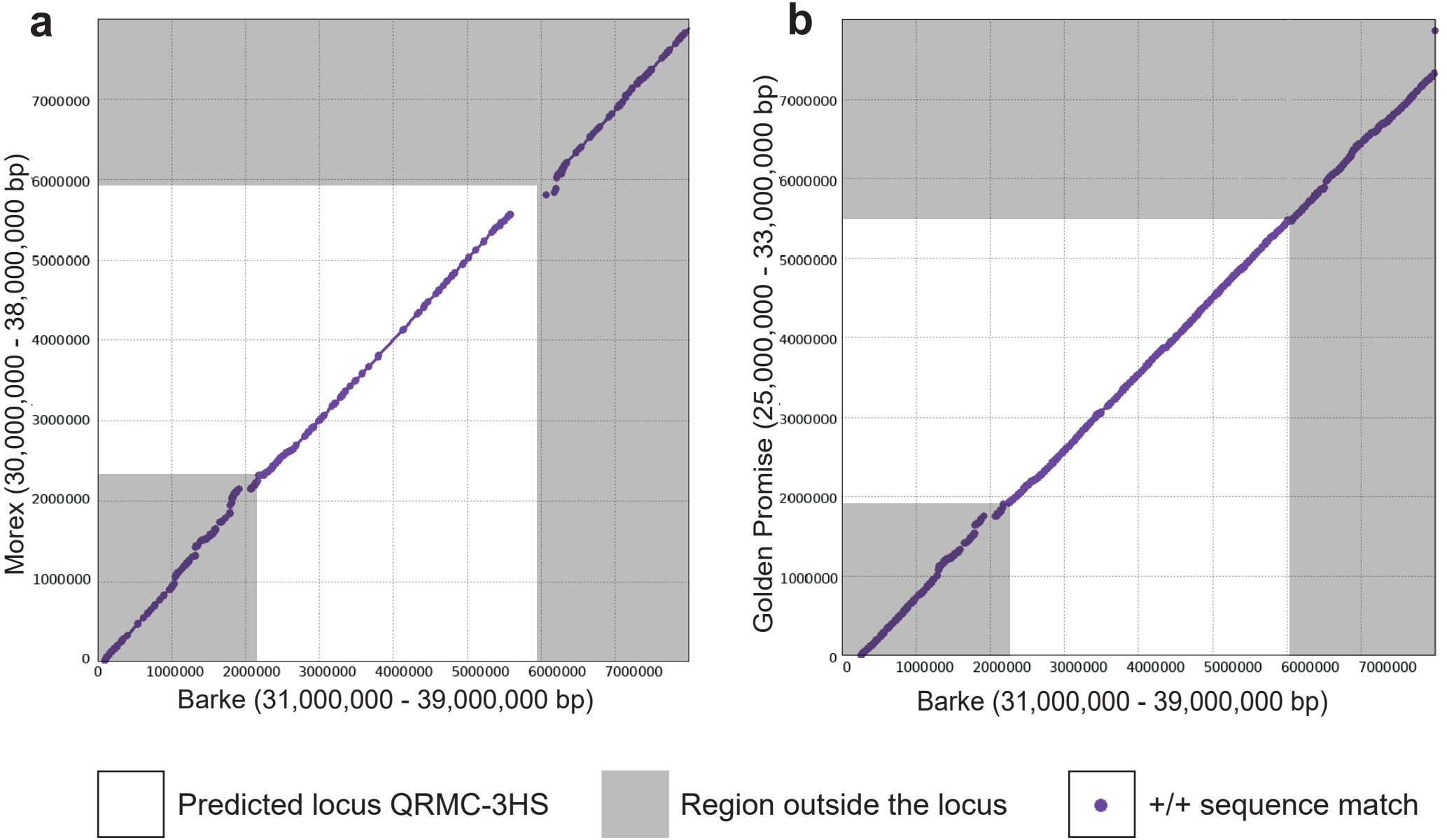

Fig. 7: The *NLR* gene is associated with genotype-dependent transcriptional and genomic variations